Eur Biophys J (2010) 39:1007–1017
DOI 10.1007/s00249-009-0503-4

ORIGINAL PAPER

Irreversible gelation of thermally unfolded proteins: structural and mechanical properties of lysozyme aggregates

Samuele Raccosta · Mauro Manno · Donatella Bulone · Daniela Giacomazza · Valeria Militello · Vincenzo Martorana · Pier Luigi San Biagio

Received: 13 February 2009 / Revised: 30 May 2009 / Accepted: 8 June 2009 / Published online: 1 July 2009

Abstract The formation of protein aggregates is important in many fields of life science and technology. The morphological and mechanical properties of protein solutions depend upon the molecular conformation and thermodynamic and environmental conditions. Non-native or unfolded proteins may be kinetically trapped into irreversible aggregates and undergo precipitation or gelation. Here, we study the thermal aggregation of lysozyme in neutral solutions. We characterise the irreversible unfolding of lysozyme by differential scanning calorimetry. The structural properties of aggregates and their mechanisms of formation with the eventual gelation are studied at high temperature by spectroscopic, rheological and scattering techniques. The experiments show that irreversible micron-sized aggregates are organised into larger clusters according to a classical mechanism of diffusion and coagulation, which leads to a percolative transition at high concentrations. At a smaller length scale, optical and atomic force microscopy images reveal the existence of compact aggregates, which are the origin of the aggregation irreversibility.

Proceedings of the XIX Congress of the Italian Society of Pure and Applied Biophysics (SIBPA), Rome, September 2008.

S. Raccosta · M. Manno (✉) · D. Bulone · D. Giacomazza · V. Militello · V. Martorana · P. L. S. Biagio
Institute of Biophysics at Palermo,
Italian National Research Council,
via U. La Malfa 153, 90146 Palermo, Italy
e-mail: mauro.manno@pa.ibf.cnr.it

S. Raccosta · V. Militello
Department of Physical and Astronomical Sciences,
University of Palermo,
via Archirafi 36, 90133 Palermo, Italy

Keywords Protein aggregation · Unfolding · Percolation · Gelation · Thermal irreversibility

Abbreviations

SALS	Small-angle light scattering
DSC	Differential scanning calorimetry
AFM	Atomic force microscopy
OD	Optical density

Introduction

The aggregation of proteins is a fundamental issue in many fields, since it is related to industrial technologies (Gosal and Ross-Murphy 2000) and clinical pathologies, such as Alzheimer disease, Creutzfeld-Jacob disease, and other neurodegenerative or systemic diseases (Prusiner 1998; Chiti and Dobson 2006). Moreover, the importance of a proper control and design of a specific protein assembly is strengthened by the growing interest in protein assemblies as new biomaterials (Zhang 2003), with potential application in food texture (Clark et al. 2001) or cellular scaffolds (Lashuel et al. 2000; Yan et al. 2006).

Here, we address the effect of thermal unfolding on protein aggregation and gelation, which is also an important functional mechanism in food proteins. By thermal unfolding, protein structure is altered in a non-specific way, e.g., by strengthening the entropic (hydrophobic) contribution with respect to the enthalpic (electrostatic) one. Heat-induced precipitation in protein solutions has long been modelled as the sequence of two processes: unfolding and aggregation (Ferry 1948). The mechanism of protein association may be attributed to molecular cross-linking (via sulphur-bridge exchange) or other interactions such as

hydrogen bonding or association of hydrophobic surfaces. In aqueous solution, the formation of protein aggregates is often related to the so-called hydrophobic effect, due to the presence of solvent and to the macromolecular conformations. In the native state, proteins are typically protected from the free-energy drive towards aggregation, while a misfolded or a (partially) unfolded conformation may determine an intermolecular effective attractive force, in order to minimise the exposure of hydrophobic residues to the polar solvent (Dill 1990). The thermodynamic stability of the native protein conformation is marginal with respect to the unfolded conformation, since it is due to a balance of different contributions such as electrostatic and hydrophobic interactions (Pace 1975; Privalov 1979). Therefore, protein aggregation is easily triggered even by mild denaturing conditions, such as a slight variation of pH or temperature (Militello et al. 2003; Vetri et al. 2007).

In this work, we present a detailed study of the aggregation and eventual gelation of a model protein, hen-egg-white lysozyme, upon thermal unfolding at high temperature. Lysozyme typically exhibits intermediate conformation under chemical or thermal unfolding (Salvetti et al. 2002; Hedoux et al. 2006). The experiments at high temperature allow us to bypass the population of such intermediate structures and the complexity of the protein conformational landscape, and thus to focus on the self-assembly of the unfolded proteins. Under the present conditions, we observe the formation of peculiar particulate morphologies, which further assemble into larger aggregates. Recent experiments suggested that the formation of particulate gels might be a generic property of all proteins and polypeptide chains (Krebs et al. 2007), as already proposed for amyloid fibrils (Chiti and Dobson 2006). Our results increase the basic comprehension of the mechanisms involved in this particular protein self-assembly. In this context, our experimental results have both an indirect biological relevance, since they clarify a case of protein self-assembly even if in a non-physiological condition, and a wide potential impact on the biotechnology community.

Lysozymes may form aggregates at physiological conditions, often by the addition of co-solvents that not only modify the solvent properties but also affect the protein structures by both indirect and direct mechanisms (Povey et al. 2007; Carrotta et al. 2009). Upon heating above 81°C at neutral pH, lysozyme undergoes unfolding and aggregation. Although thermally induced unfolding may be reversible for some proteins (Gray et al. 2001), at high temperature the denaturation is often irreversible due to the concurrent aggregation. In our conditions, the unfolding-driven aggregation of lysozyme is due to hydrophobic effect and not to the breakage and exchange of the sulphur bridges, which requires the addition of a reducing agent, such as dithiothreitol (Nayakawa and Nakamura 1986; Yan et al. 2006). Indeed, the protein hydrophobic surface exposed to the solvent changes rapidly between 75 and 85°C (Kato et al. 1986; Van der Plancken et al. 2006), while the secondary structures in the same temperature range are altered only upon long incubation (Nohara et al. 1999).

The unfolding process and its irreversibility were studied by differential scanning calorimetry (DSC). We studied the structural and mechanical properties of lysozyme aggregates by small-angle light scattering (SALS), oscillatory and rotatory rheological techniques, optical microscopy and atomic force microscopy (AFM). By time-resolved optical-density (OD) measurements, we found that the aggregation process proceeds via a second-order reaction scheme and at high concentrations ends up in macroscopic gelation. Also, under the present experimental conditions, the thermal unfolding of lysozyme is irreversible, due to the formation of compact irreversible aggregates, with a size from a few tens of nanometers to a few micrometers, as observed in other protein systems (Krebs et al. 2007). The structural and mechanical properties of these aggregates seem independent of the initial protein concentration. Such microscopic aggregates assemble into large fractal clusters, which give gel-like properties to the sample. Upon increasing concentration, the number of clusters increases up to a percolative phase transition and to the macroscopic gelation.

The present experiments highlight the hierarchical structure of lysozyme-aggregated samples and gels and mark the different properties of the aggregates on the microscopic time scale, where irreversibility is built in, and those on a mesoscopic scale, which determine the macroscopic and gel-like behaviour.

Materials and methods

Sample preparation

Lysozyme is a globular protein with an approximately ellipsoidal shape, a molecular mass of 14.3 kDa (129 residues) and an isoelectric point of 11.2 (Tanford and Epstein 1954). Hen-egg-white lysozyme (three times crystallised, dialyzed and freeze-dried) was purchased from Sigma Chemical and used without further purification. The buffer solution was 0.1 M phosphate in Millipore Super-Q water, at pH 7.0. Lysozyme solutions were freshly prepared by the following procedure. Protein powder was directly dissolved in buffer solution. Sample was centrifuged at 800*g* for 2 min to remove air bubbles and small amounts of undissolved material and filtered into a cell through a 0.2-μm Sartorius syringe filter. Sample concentration was determined by UV absorption

spectroscopy measurements (Shimadzu UV-2401PC). The extinction coefficient for lysozyme at 280 nm was taken as $\varepsilon_{280\text{nm}} = 2.46\ \text{cm}^{-1}\ (\text{mg/ml})^{-1}$.

Differential scanning calorimetry

Differential scanning calorimetry (DSC) experiments were performed by using a Hart Scientific Calorimeter coupled with a transputer-driven control unit (Bulone et al. 1994). To begin, 270 µl of sample was introduced in a 1-ml steel cell; the same quantity of buffer solution was inserted in a reference cell. Both cells were kept under nitrogen laminar flow to avoid air water condensation. Measures were performed on concentrated samples (10–60 mg/ml) with a scan rate of 8°C/h and a temperature range of 25–85°C. The excess thermal capacity C_p^{exc} is calculated from the calorimetric profile by subtraction of a quadratic baseline, which is obtained by fitting the calorimetric curve neglecting the peak.

Small-angle light scattering

Small-angle light scattering (SALS) structure functions were obtained by using a light-scattering apparatus built in our laboratory (Manno et al. 2007) and equipped with a charge-coupled device Pulnix TM765 camera and an He–Ne laser operating at a wavelength of 632.8 nm. Measurable intensities span a wide dynamic range (from 1 to 3×10^5, in arbitrary units), thanks to a software integration of multiple exposure times (from 1/60 to 1/10,000 s). After background subtraction, reliable measurements could be made over a range of scattering angles from 0.1 to 11°, with a maximum resolution of 0.01°, corresponding to scattering vector magnitudes between 0.02 and 2 μm^{-1}. The measurements were done into quartz cuvettes with an optical path of 2 mm, at room temperature. In order to avoid multiple scattering in aggregated samples, we diluted the sample with the buffer solution to obtain a transmittance $\geq$90%. We checked that the profile of the structure functions was not altered by successive dilutions, once multiple scattering was supressed. Very high dilutions were avoided, since a loss of material was detected (data not shown).

Optical density

Time-resolved optical density (OD) experiments were performed immediately after sample preparation at the wavelength of 632.8 nm, at the temperature of 81°C and at different lysozyme concentrations. Samples were placed in a quartz cell (1 cm optical path), inserted into a thermostated cell compartment of an UV-VIS spectrophotometer (Jasco V-530). The temperature was controlled within 0.05°C with a thermostated recirculating bath.

Optical microscopy

At the end of the turbidity experiments, a drop of the solution was put on a glass slide for imaging with an inverted microscope with colour-corrected infinity optical system (MOTIC AE21), equipped with 1.3 Mpixel digital camera.

Atomic force microscopy

At the end of the turbidity experiments, 10 µl of the incubated solution was diluted into 1 ml buffer solution, quenched to room temperature and used for atomic force microscopy (AFM) experiments. A few microliters of the solution were dropped onto a freshly cleaved mica substrate. After a few minutes, the sample was washed dropwise with Millipore SuperQ water and then dried with a gentle stream of dry nitrogen. The drying is expected to remove most of the surface water, while keeping the protein aggregates substantially hydrated locally. Images of the protein aggregates were recorded with a Multimode Nanoscope V Atomic Force Microscope (Veeco Instruments, Santa Barbara, CA, USA), operating in Tapping Mode. We used rigid cantilevers (model RFESP) with resonance frequency of about 85 kHz and equipped with single crystal silicon tips with a nominal radius of curvature of 5–10 nm. Typical scan size was $500 \times 500\ \text{nm}^2$ (512×512 points), and line scan rate was 0.5 Hz. The analysis of AFM images was done by using the open-source software Gwyddion.

Rheological experiments

Samples incubated at 81°C were pipetted onto the plate (thermally controlled by a Peltier device) of a stress-controlled rheometer (AR1000, T.A. Instruments UK). The geometry used was a 40-mm titanium cone with an angle of less than 1° and a 26-µm truncation length (T.A. Instruments). Each excess sample was blotted away with filter paper, and paraffin oil (GPR grade, BDH, UK) was layered around exposed regions. A solvent-trap cover-slip was also used to prevent evaporation. Viscoelastic spectra were measured at 20°C in the range between 0.1 and 200 rad s^{-1}, with a strain of 0.01. Viscosities were also measured at 20°C as a function of shear rate (from 1 to 1,000 s^{-1}).

Results and discussion

Irreversible unfolding and aggregation

The thermal unfolding of lysozyme in neutral solution was studied by differential scanning calorimetry at different

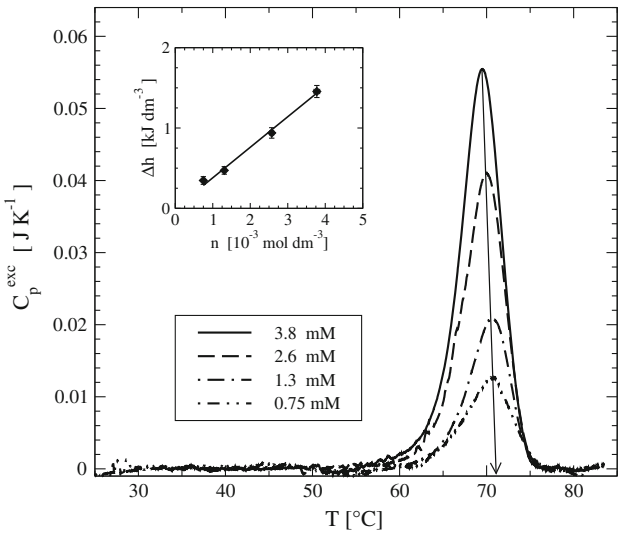

Fig. 1 Excess thermal capacity thermograms at different lysozyme concentrations (as specified in the figure). The *arrow* is a guide for the eyes through the peak maxima and towards the extrapolation at infinite dilution $T_{1/2} = 71.1$°C. *Inset* Enthalpy density versus molar concentration. The *solid line* is a linear fit

protein concentrations. The samples were loaded into the cells at 25°C and brought to 85°C with a scan rate of 8°C/h. Then the samples were rapidly cooled to 25°C at 0.6°C/min, and a second upward scan was performed at the same scan rate of 8°C/h. The calorimetric profiles of the excess thermal capacity C_p^{exc} in the first upward scan are shown in Fig. 1 for different lysozyme concentrations. A single endothermic peak, related to protein unfolding, is present in each scan. In the second scan (which is not shown to not overcrowd the picture), the peak is completely missing, providing evidence of the irreversibility of thermal unfolding.

In some cases, lysozyme native structure can be restored after thermal denaturation (Sabulal and Kishore 1995; Nohara et al. 1999), while in other ones the unfolding is irreversible (Privalov 1979). In general, calorimetric irreversibility can be ascribed either to an incorrect refolding of monomers (misfolding) or to the aggregation process. In our case both processes are likely involved. Indeed, the second upward scan is expected to be not flat when aggregation is irrelevant. The second scan would be comparable to the first one if proteins were correctly refolded, or it would be slightly different if proteins were misfolded. In the present experiments, we observe a flat profile in the second upward scan. Therefore, the irreversibility can be ascribed to the aggregation process. The unfolded proteins are stuck into supramolecular aggregates and not allowed to recover their native structure.

Experiments performed under similar conditions, but without salt in the solution (pure water), revealed a non-null DSC signal upon reheating the sample (Yan et al. 2006), due to a reduced aggregation rate. The main role of salt is to screen the protein charge. Lysozyme at pH 7 has a net positive charge of 7.5 electron charge (Tanford and Epstein 1954; Rosch and Errington 2007). It is reasonable that in this case the electrostatic repulsion inhibits the aggregation (Dill 1990). Analogously, the aggregation process is inhibited within a few days at acid pH, that is at high protein net charge (Arnaudov and de Vries 2005). In our experimental conditions, the presence of salt screens the electric charge and enhances the aggregation rate.

The aggregation process is typically an exothermic process (Azuaga et al. 2002; Barone et al. 1992). However, the heat exchange due to aggregation is not comparable to that of molecular unfolding. Indeed, the enthalpy density Δh associated with the overall process, calculated as the area under the C_p^{exc} curves divided by the sample volume, depends linearly upon the molar concentration n (inset of Fig. 1), confirming that the endothermic peak is related to unfolding, and it is only marginally distorted by aggregation. A footprint of aggregation is anyhow evident in the small shift of the midpeak temperature $T_{1/2}$ upon increasing concentration. The actual midpoint temperature can be estimated by a linear extrapolation of such temperatures to infinite dilution, which yields the value of $T_{1/2} = 71.1$°C (arrow in Fig. 1). The slope of the plot in the inset of Fig. 1 gives the molar enthalpy associated with the unfolding process: $\Delta H_U = 380 \pm 20$ kJ mol^{-1}. This value is consistent with previous experiments on lysozyme thermal denaturation (Claudy et al. 1992). The calorimetric profile is consistent with an unfolding transition between two states (Privalov 1979). However, an unsolved question in calorimetry is whether all the proteins are in the same conformational state at a given temperature or they are statistically distributed between at least two main states (native and unfolded).

The aggregation process

The aggregation of lysozyme was studied at 81°C. At such a high temperature and concentration, the protein is unfolded (see Fig. 1) as elicited by DSC experiments, although it contains a considerable amount of secondary structure (Nohara et al. 1999; Mine et al. 1990). In this condition, aggregation occurs starting in the very early stages (Nohara et al. 1999). We performed optical density (OD) kinetic experiments at different lysozyme concentrations (Fig. 2). The OD values reach a plateau at the end of the kinetics, when the aggregation process is complete. In some cases, precipitation of larger aggregates occurs, sometimes affecting the final plateau value. The curves in Fig. 2 exhibit a similar shape if one excludes the early kinetics at the highest protein concentrations, which lie within the thermalisation time. Such a similarity indicates

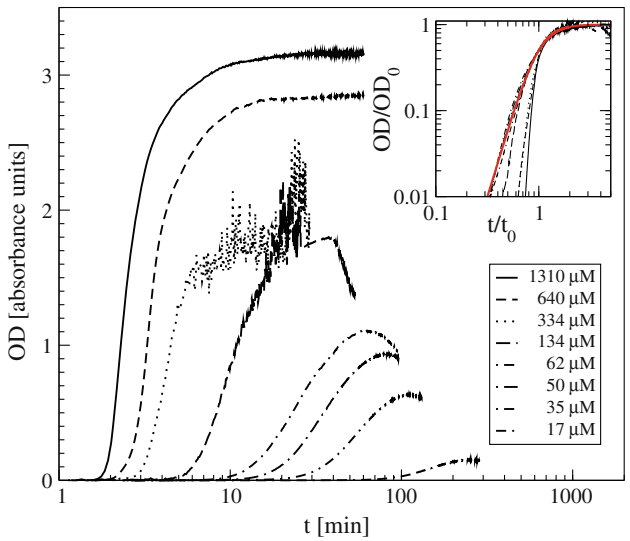

Fig. 2 Kinetics of optical density of lysozyme solutions at 81°C at different concentrations (as specified in the figure). *Inset* OD kinetics rescaled by the parameters OD_0 and t_0, as indicated in the text. The *bold coloured curve* is a fit to Eq. 1

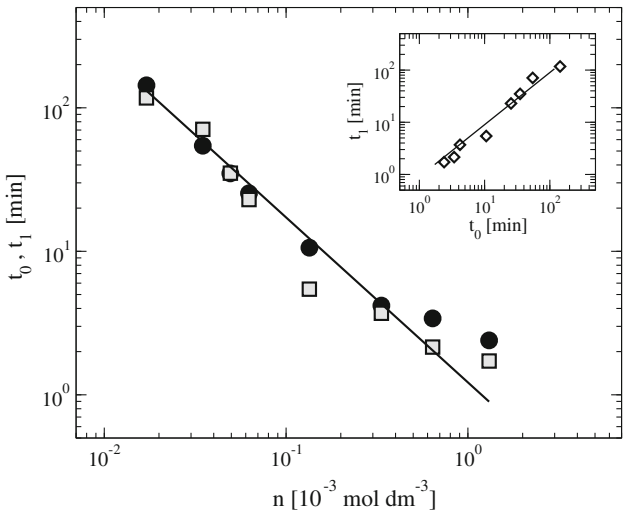

Fig. 3 Characteristic times of OD kinetics. *Circles* t_0, *squares* t_1, *solid line* power law fit $t \approx n^{-1.15}$. *Inset* Linear correlation between the two characteristic times

that the same mechanism operates at all the concentrations. Indeed, the OD curves may be rescaled by identifying a characteristic time t_0 and a plateau value OD_0, as shown in the inset of Fig. 2. The bold coloured curve in the inset of Fig. 2 is a sigmoidal Hill curve:

$$\frac{\mathrm{OD}_0}{\mathrm{OD}} = 1 + \left(\frac{t_0}{t}\right)^n \qquad (1)$$

The latter expression with an exponent $n = 4$ reproduces approximatively the growth of the OD signal at all the concentrations. At very high concentrations, the initial part of the kinetics is not reliable since the main growth occurs during the sample thermalisation. In the present experiments, the presence of a final plateau is not merely due to monomer or aggregate consumption (Flyvbjerg et al. 1996). Other effects, such as multiple scattering or mesoscopic gelation, may affect the late stages (Baussay et al. 2004). Thus, in order to identify a more reliable characteristic time related to the onset of the aggregation process, we considered the characteristic time t_1, defined as the time necessary to reach the small threshold of 0.05 absorbance units.

The two characteristic times t_0 and t_1 are displayed in Fig. 3. The inset highlights that the two quantities are linearly correlated. The characteristic time of the kinetics exhibits an inverse quasi-linear dependence upon molar concentration. More precisely, the data can be fit with a power law $t \approx c^{-1.15}$ (Panouille et al. 2004). A linear dependence between the aggregation rate and the protein concentration calls for a second-order reaction kinetics, where the growth is determined by the coalescence of two objects (two monomers, two aggregates, one monomer and one aggregate, and so on) (Nohara et al. 1999).

The structure of aggregates

The morphology of lysozyme aggregates formed after incubation at 81°C was observed by optical microscopy. Figure 4 displays some typical aggregates. They are large clusters with a size spanning from a few tens of micrometers to hundreds of micrometers, made of smaller micron-sized units. The heterogeneity of shapes and sizes is a clear result of a kinetic coagulation process.

In order to get more quantitative, and statistically significant, information about the structural properties of such aggregates, we performed SALS measurements on incubated samples at different concentrations (Fig. 5). In each circumstance, the incubation time is taken as the time when the OD signal reaches a plateau value. At the highest concentration in Fig. 5, we clearly observe a power-law dependence in the range of scattering vector between 0.1 and 1 μm^{-1}. The curve is bent at higher scattering vectors. Such a profile of the structure function is typical of clusters having a radius of gyration R_g of tens of micrometers (consistent with microscopy images), which are made from smaller units with a size R of a few microns. The shape of the structure functions in the high range of scattering vectors q is substantially conserved at all concentrations, while the power-law region is restricted to a limited range by lowering the protein concentration, showing that the observed size of clusters R_g is smaller at lower concentrations.

We fit the scattered intensity data $I(q)$ by using a hierarchical form factor that includes a form factor for the small compact object $P(q)$ and a structure factor for the large cluster $S(q)$ (Carrotta et al. 2007):

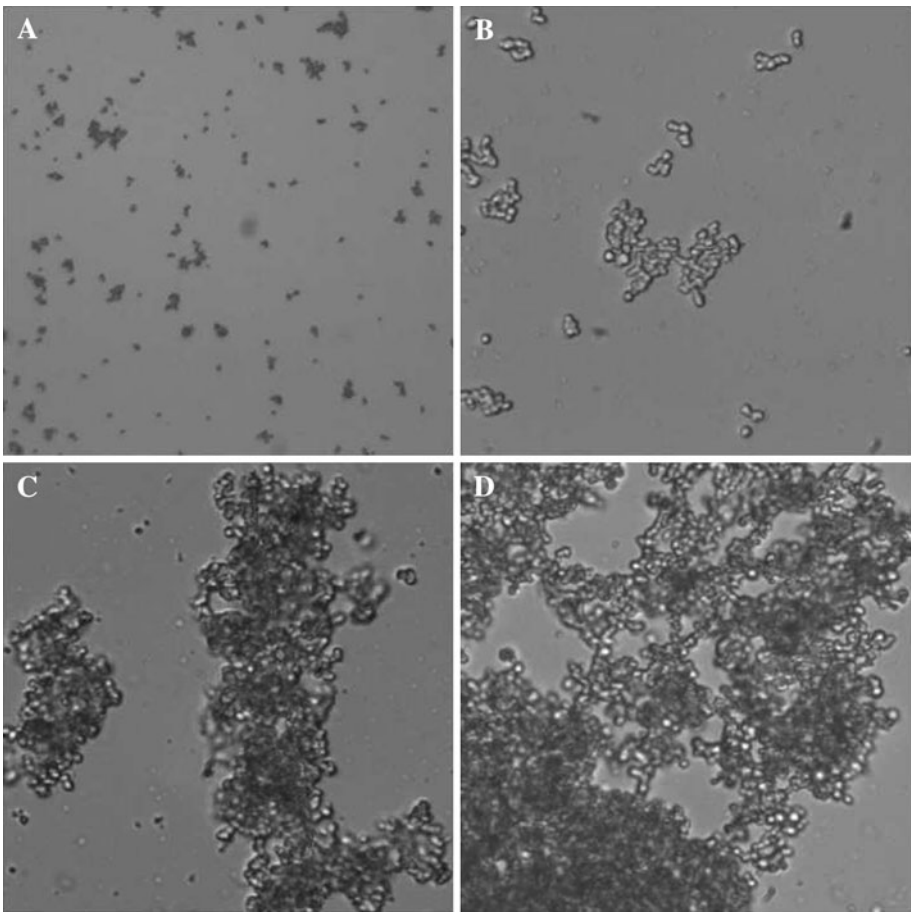

Fig. 4a–d Optical microscopy images of a lysozyme solution at different concentrations after incubation at 81°C. **a** c = 50 μM, side length = 336.5 μm (10×); **b** c = 50 μm, side length = 91.2 μm (40×); **c** c = 134 μm, side length = 91.2 μm (40×); **d** c = 334 μm, side length = 91.2 μM (40×)

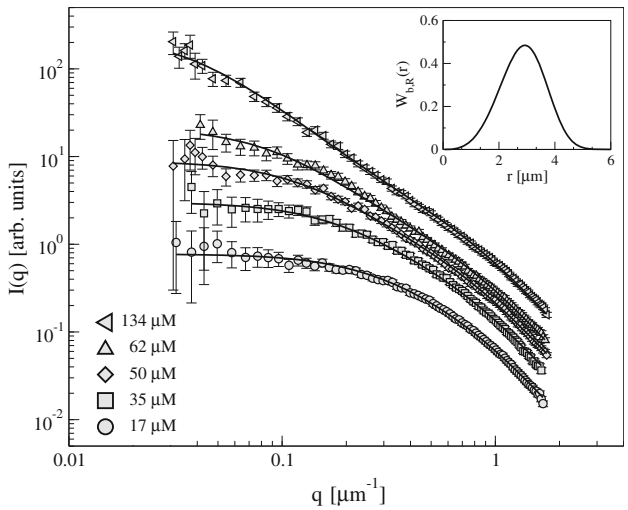

Fig. 5 Scattered intensity (in arbitrary units) of lysozyme solutions after incubation at 81°C at different concentrations (as specified in the figure). The samples are diluted to obtain a transmittance of about 90%. The lines are best fits to Eqs. 2, 3, 4. *Inset*: Distribution function $W_{b,R}(r)$ of the radii of the small aggregates as to Eq. 4

$$I(q) = S(q)P(q) \tag{2}$$

Guided by the microscopy images we used a general function $S(q)$ developed to model fractal aggregates with fractal dimension d and radius of gyration R_g, made from m smaller compact objects of size R (Nicolai et al. 1996):

$$S(q;R_g,R,d) = \frac{1}{m}\left[1 + \frac{m-1}{\left[1+(\xi q)^2\right]^{\frac{d-1}{2}}}\frac{\sin((d-1)\mathrm{atan}(\xi q))}{(d-1)\xi q}\right] \tag{3}$$

where $\xi = R_g/[d(d+1)/2]^{0.5}$ is the correlation length related to a cluster, and m is the number of small units that are assembled in one cluster: $m = 1 + \Gamma(d+1)(\xi/R)^d$, where $\Gamma(x)$ is the Gamma function.

The latter expression introduces a very minimalistic model for the structure of aggregates. Indeed, we obtain only three parameters: the size of clusters R_g, the size of the constituent units R, and the fractal dimension d of clusters, which is essentially a measure of the packing of the small units into the large aggregates. In the present case, the value of $d = 2.0$ has been fixed to the best fit value of the curve at the highest concentration. The best-fit values for the radius of gyration R_g of large clusters are 6.2, 9.3, 13, 18 and 45 μm respectively for the concentrations c = 17, 35, 50, 62 and 134 μM, consistent with microscopic observations.

The form factor of the small units $P(q)$ may be fit by using either the well-known expression for hard spheres or a simplified Fisher-Burford expression $F_D(Rq)$, used to extend the Guinier range (Nicolai et al. 1996). We fit the data of Fig. 5 by allowing a polydispersity in the radius R of the smaller units and by using a Weibull distribution function $W_{b,R}(r)$ with average R (Carrotta et al. 2007; Pedersen 1993).

$$P(q) = \int_0^\infty W_{b,R}(r) F_D(rq) \mathrm{d}r$$

$$W_{b,R}(r) = b\left[\frac{\Gamma(\frac{1}{b}+1)}{R}\right]^b r^{b-1} \exp\left\{-\left[\frac{r\Gamma(\frac{1}{b}+1)}{R}\right]^b\right\} \qquad (4)$$

$$F_D(rq) = \left[1 + \frac{2}{3D}(rq)^2\right]^{\frac{-D}{2}}$$

The parameter b is a measure of radii polydispersity. The best-fit parameters are $R = 2.85$ μm, $b = 4$ and $D = 3$. The value $D = 3$ marks the presence of very compact aggregates.

By optical microscopy and SALS, we are addressing the structural properties of lysozyme aggregates at a microscopic length scale. In order to extend the structural details to a smaller length scale, we performed atomic force microscopy experiments on lysozyme aggregates formed after incubation at 81°C. Figure 6 displays some typical aggregates. They are compact aggregates with a typical size of a few tens of nanometers. Their aspect mirrors the morphology of the aggregates found at larger length scales by optical microscopy.

Mechanical properties of aggregates

After incubation at 81°C, lysozyme solutions became viscous as expected when large clusters form. At concentrations higher than 350 μM, the samples exhibited no macroscopic flow, and they appeared as turbid macroscopic gels. The viscoelastic properties of such incubated samples were investigated by measuring the viscoelastic spectra at the different concentrations and at 20°C. The storage G' and loss G'' moduli are shown in Fig. 7. The most evident result is that at the high concentrations, the viscoelastic spectra are almost flat, and they have much higher values than the spectra at the lower concentration. This is essentially a quantitative confirmation of the visual inspection of firm gels at the higher concentrations.

Also in the set of lower concentrations, both the storage and loss spectra display a power-law behaviour with about the same exponent $n = 0.5$ in the range of strain frequencies ω between 1 and 10 rad s^{-1}. We can affirm that, in this frequency range, the samples exhibit a gel-like behaviour (Ferry 1980; Winter and Chambon 1986). At

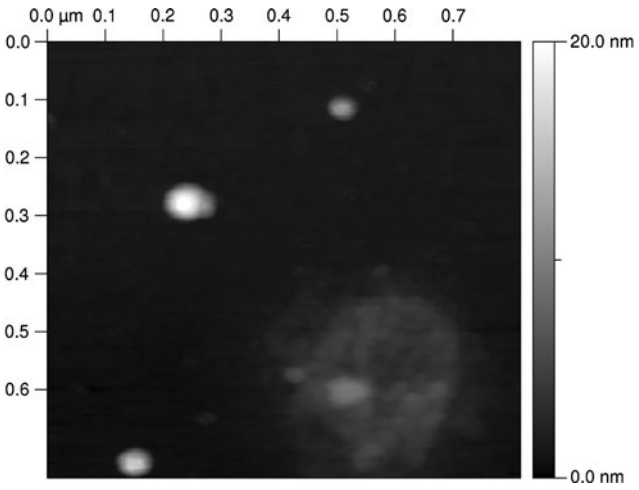

Fig. 6 Atomic force microscopy images of a 35 μM lysozyme solution after incubation at 81°C. The side length is 800 nm. The *side bar* indicates a grey tone mapping at the vertical axis

lower frequencies, the moduli are bent towards lower values, that is they recover the typical liquid behaviour and display macroscopic flow. The shapes of the viscoelastic moduli are similar to the so-called Rouse model, which describes the mechanical relaxation of a sample of non-entangled clusters (Rouse 1953). At higher frequencies, the storage modulus G' rises with an asymptotic square dependence upon the frequency. We fit the data by using the following ad-hoc expressions:

$$G' = G'_0 \frac{(\tau'_0\omega)^2}{1+(\tau'_0\omega)^2}\left[1+(\tau'_0\omega)^2\right]^{\frac{n}{2}} + G_1(\tau_1\omega)^2 \qquad (5)$$

$$G'' = G''_0 \frac{(\tau''_0\omega)}{1+(\tau''_0\omega)^2}\left[1+(\tau''_0\omega)^2\right]^{\frac{n+1}{2}} + \eta_b\omega \qquad (6)$$

In the first term of the latter two equations, the fraction is the usual expression for a Maxwell liquid (Ferry 1980), while the expression in square brakets, with the parameter $n = 0.5$ in the exponent, is a suitable term that reproduces the Rouse behaviour. In the three highest concentrations, the spectra are more flat with $n = 0.20 \pm 0.01$. The parameter G'_0 and G''_0, and τ'_0 and τ''_0 were left free in the fit, and they have consistent values. The average values $G_0 = (G'_0 + G''_0)/2$ and $\tau_0 = (\tau'_0 + \tau''_0)/2$ are displayed in Fig. 9. The second term in Eq. 6 is introduced to include the effect of bulk viscosity η_b, which is of the order of water viscosity, i.e. $\eta_b = 10^{-3}$ Pa s. In these measurements, the addition of this term is almost irrelevant, since the loss moduli have quite high values. The second term in Eq. 5 for the storage modulus is included to fit the increase of G' at high frequencies. Interestingly, the parameter $G_1\tau_1^2$ is the same at all the concentrations and has a value of 10^{-3} Pa s^2. This suggests the existence of a relaxation

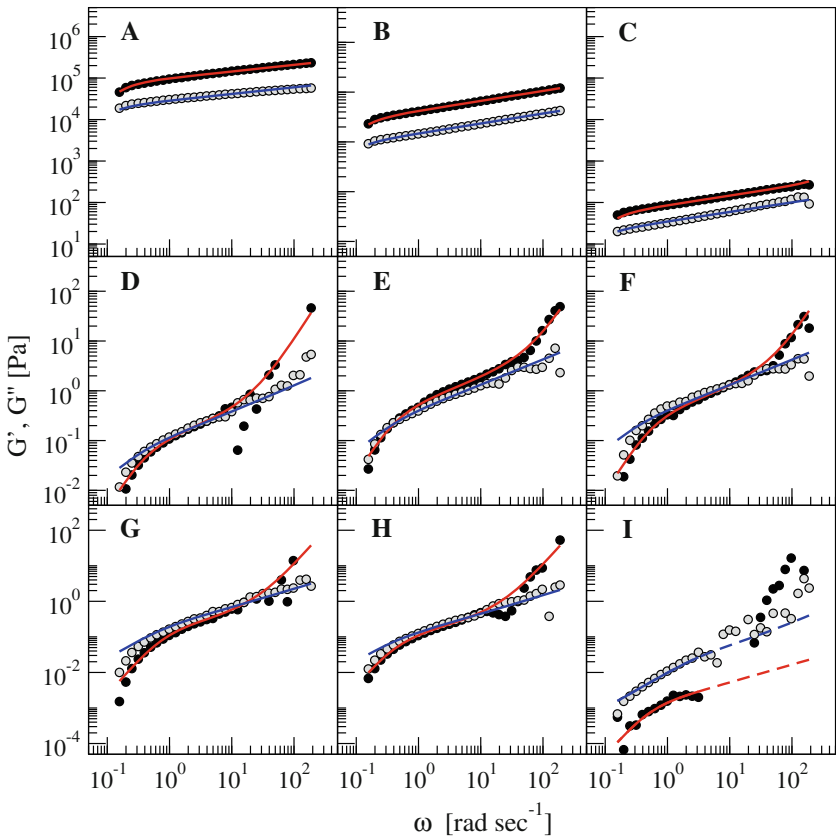

Fig. 7a–i Viscoelastic spectra of lysozyme solutions after incubation at 81°C at different concentrations: storage modulus G' (*black circles*), loss modulus G'' (*grey circles*). The lines are best fits to Eqs. 5, 6. **a** 4,000 μM, **b** 1,310 μM, **c** 640 μM, **d** 334 μM, **e** 134 μM, **f** 62 μM, **g** 50 μM, **h** 35 μM, **i** 17 μM

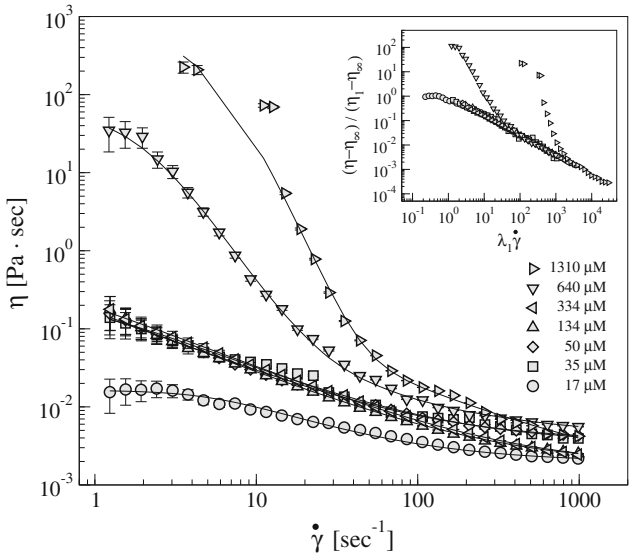

Fig. 8 Viscosity versus shear rate of lysozyme solutions after incubation at 81°C at different concentrations (as specified in the figure). The *solid curves* are fits to Eq. 7. *Inset* Viscosity curves rescaled as indicated in the axes

process at small time scales and hence at small length scales, which occurs at all the concentrations (Puertas et al. 2007).

This observation is also consistent with the results of viscosity experiments. We measured viscosity as a function of shear rate on the incubated samples. We found a typical shear-thinning behaviour (Fig. 8). The curves of Fig. 8 were fit by the well-known Carreau expression (Barnes et al. 1989). At concentrations higher than 350 μM, when the flow is completely inhibited, we added a second term. The data of Fig. 8 were fit with the following expression, which extends the Carreau model:

$$\eta = \eta_\infty + (\eta_1 - \eta_\infty)\left[1 + (\lambda_1\dot{\gamma})^2\right]^{\frac{n_1-1}{2}} + \eta_2\left[1 + (\lambda_2\dot{\gamma})^2\right]^{\frac{n_2-1}{2}} \quad (7)$$

The latter expression reproduces the shear thinning with the exponent $n_1 = 0.2$ and yields two useful parameters: the zero-shear-rate viscosity $\eta_0 = \eta_1 + \eta_2$, and the infinite-shear-rate viscosity η_∞. The parameter λ_1 is a characteristic time. Its value is of the order of a few seconds, consistent with the values of τ measured in the viscoelastic spectra. The curves in Fig. 8 have been rescaled by using the fit parameters λ_1, η_1 and η_∞. All the curves collapse into the same master curve, with the exception of the second relaxation process present at the two highest concentrations.

The zero-shear-rate viscosity η_0 has the same concentration dependence of the elastic modulus G_0, as shown in Fig. 9. Indeed these two parameters reflect the macroscopic gel behaviour of the samples. On the other hand, the infinite-shear-rate viscosity η_∞ does not depend upon protein

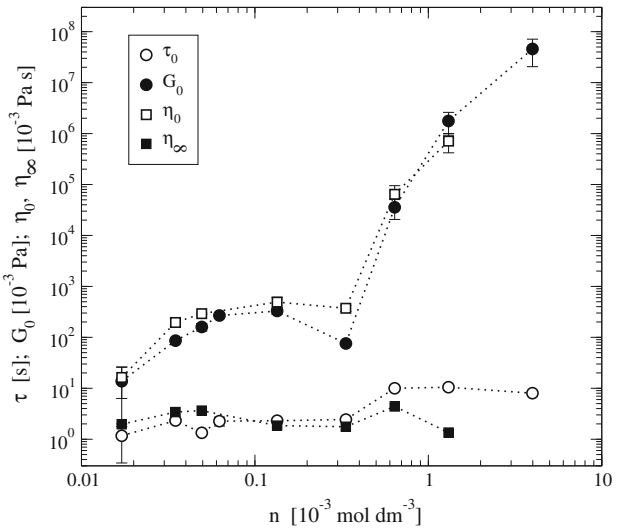

Fig. 9 Rheological parameters versus protein concentrations: τ_0 (*empty circles*), G_0 (*full circles*), η_0 (*empty squares*), η_∞ (*full squares*)

concentration (Fig. 9). This highlights the fact that on a microscopic length scale, the mechanical properties are similar in the entire range of studied concentrations. In general, the viscosity of a colloidal solution would exhibit a linear dependence on concentration. However, since the intrinsic viscosity is typically on the order of a few units, the concentration dependence can be confidently observed at high volume fractions (Rueb and Zukoski 1998). In the present experiments, the volume fractions are below 0.04, and we do not expect to observe any concentration dependence. The same concentration-independent behaviour was found in the structure and size of small micron-sized aggregates that form larger clusters. At high shear rate, the large clusters are likely disassembled and the small compact irreversible aggregates remain at all the concentrations. At low shear rate, the cluster structure and size depend upon the initial concentration, as found in the SALS structure functions.

In Fig. 9, we observe that, while the mechanical properties of small aggregates do not depend upon concentration (quasi-constant η_∞), the elastic modulus and the zero-shear-rate viscosity dramatically increase above the threshold of 340 μM lysozyme concentration. This reveals that the formation of a macroscopic gel is due to the percolation of large clusters, which occurs above a given threshold concentration.

Conclusions

Lysozyme is known to self-assemble under certain thermodynamic and environmental conditions to form different supramolecular structures. At moderately acid pH and ionic strength, lysozyme solutions may undergo a liquid-liquid phase separation (Muschol and Rosenberger 1997; Manno et al. 2003) which facilitates the formation of crystals (tenWolde and Frenkel 1997; Poon et al. 2000). Also, lysozyme is able to assemble into amyloid fibrils upon heating at low pH (Krebs et al. 2000; Arnaudov and de Vries 2005), or upon addition of alcohol (Cao et al. 2004). Proteins can also undergo amorphous aggregation and gelation (Gosal and Ross-Murphy 2000; Navarra et al. 2009). This type of aggregation is closely studied in food science and bioengineering (Clark et al. 2001).

In the present work, we studied the aggregation of lysozyme at 81°C, in neutral phosphate buffer solution (pH 7). At this temperature the protein is unfolded. By DSC we have measured the enthalpy related to the unfolding process: $\Delta H = 380 \pm 20$ kJ mol^{-1} (Fig. 1). Also, we have observed that thermal unfolding is made irreversible by protein aggregation.

The aggregation of unfolded lysozyme has been studied by time-resolved optical-density experiments (Fig. 2). The aggregation proceeds via second-order reaction kinetics, that is by simple diffusion and coalescence of two macromolecular units, either unfolded monomers or aggregates (Fig. 3).

At a submicron length scale, proteins assemble into compact ellipsoidal objects. The size of such aggregates ranges from a few tens of nanometers to a few microns, as revealed by AFM (Fig. 6) and optical microscopy imaging (Fig. 4), as well as by SALS measurements (Fig. 5). Such aggregates are the very cause of the irreversibility of thermal unfolding. They do not disassemble either upon cooling or upon dilution. The smooth and compact appearence of such aggregates is reminiscent of the particulate protein aggregates recently found in many protein systems (Krebs et al. 2007).

The microscopy and scattering experiments also revealed that such aggregates are organised into larger fractal clusters, whose size increases with increasing concentration. At protein concentrations below 350 μM, the samples containing these clusters are able to flow on the time scale of a few seconds, while at lower time scales they exhibit a gel-like behaviour. Their properties are akin to that of the Rouse model, for non-entangled clusters, as shown by the viscoelastic spectra (Fig. 7). Also, such samples undergo shear-thinning upon increasing the shear rate (Fig. 8). At protein concentrations above 350 μM, the samples undergo macroscopic gelation and change their mechanical properties. Both the elastic modulus and the zero-shear-rate viscosity increase dramatically above that threshold concentration, highlighting a percolative phase transition. Interestingly, the mechanical properties at a microscopic length and time scale do not depend upon concentration, as confirmed by the infinite-shear-rate viscosity (Fig. 9).

In conclusion, we have determined the structural and mechanical properties of unfolded lysozyme aggregation. Irreversible aggregates are formed with the same properties at all the concentrations. These aggregates assemble into fractal clusters. Above a threshold concentration, the percolation of such clusters causes the macroscopic gelation of the samples.

Acknowledgments We thank R. Carrotta, G. Bellavia, A. Cupane, A. Emanuele, M. Leone, R. Noto and V. Vetri for relevant discussions and collaborations. We thank V. Foderà for the help in the use of the AFM instruments. This work was partially supported by the Italian National Research Council through the project "Intermolecular interaction in protein metastable solution".

References

Arnaudov LN, de Vries R (2005) Thermally induced fibrillar aggregation of hen egg white lysozyme. Biophys J 88(1):515–526

Azuaga AI, Dobson CM, Mateo PL, Conejero-Lara F (2002) Unfolding and aggregation during the thermal denaturation of streptokinase. Eur J Biochem 269:4121–4133

Barnes HA, Hutton JF, Walters K (1989) An introduction to rheology. Elsevier, Amsterdam

Barone G, Giancola C, Verdoliva A (1992) Dsc studies on the denaturation and aggregation of serum albumins. Thermochim Acta 199:197–205

Baussay K, Bon CL, Nicolai T, Durand D, Busnel J-P (2004) Influence of the ionic strength on the heat-induced aggregation of the globular protein *b*-lactoglobulin at pH 7. Int J Biol Macromol 34:21–28

Bulone D, Fornili LG, Fornili SL, Lapis M, San Biagio PL (1994) Transputer-based upgrading of a differential scanning calorimeter. Meas Sci Technol 5:1443–1447

Cao A, Hu D, Lai L (2004) Formation of amyloid fibrils from fully reduced hen egg white lysozyme. Protein Sci 13:319–324

Carrotta R, Barthès J, Longo A, Martorana V, Manno M, Portale G, San Biagio PL (2007) Large size fibrillar bundles of the Alzheimer amyloid β-protein. Eur Biophys J 36:701–709

Carrotta R, Manno M, Giordano FM, Longo A, Portale G, Martorana V, San Biagio PL (2009) Protein stability modulated by a conformational effector: effects of trifluoroethanol on bovine serum albumin. Phys Chem Phys 11:4007–4018

Chiti F, Dobson CM (2006) Protein misfolding, functional amyloid, and human disease. Annu Rev Biochem 75:333–366

Clark A, Kavanagh G, Ross-Murphy S (2001) Globular protein gelation-theory and experiment. Food Hydrocolloids 15:383–400

Claudy P, Létoffé JM, Bayol A, Bonnet MC, Maurizot JC (1992) Denaturation versus pH of lysozyme and biosynthetic human growth hormone by differential scanning calorimetry and circular dichroism: a comparative study. Thermochim Acta 207:227–237

Dill KA (1990) Dominant forces in protein folding. Biochemistry 29(31):7133–7155

Ferry JD (1948) Protein gels. Adv Protein Chem 4:1–78

Ferry JD (1980) Viscoelastic properties of polymers. Wiley, New York

Flyvbjerg H, Jobs E, Leibler S (1996) Kinetics of self-assembling microtubules: an "inverse problem" in biochemistry. Proc Natl Acad Sci USA 93:5975–5979

Gosal W, Ross-Murphy SB (2000) Globular protein gelation. Curr Opin Colloid Interface Sci 5:188–194

Gray KA, Richardson TH, Kretz K, Short JM, Bartnek F, Knowles R, Kan L, Swanson P, Robertson DE (2001) Rapid evolution of reversible denaturation and elevated melting temperature in a microbial haloalkane dehalogenase. Adv Synth Catal 343:607–617

Hedoux A, Ionov R, Willart J-F, Lerbret A, Affouard F, Guinet Y, Descamps M, Prevost D, Paccou L, Danede F (2006) Evidence of a two-stage thermal denaturation process in lysozyme: a Raman scattering and differential scanning calorimetry investigation. J Chem Phys 124:014703

Kato A, Fujimoto K, Matsudomi N, Kobayashi K (1986) Protein flexibility and functional properties of heat-denatured ovalbumin and lysozyme. Agric Biol Chem 50:417–420

Krebs M, Wilkins D, Chung E, Pitkeathly M, Chamberlain A, Zurdo J, Robinson C, Dobson C (2000) Formation and seeding of amyloid fibrils from wild-type hen lysozyme and a peptide fragment from the beta-domain. J Mol Biol 300:541–549

Krebs MRH, Devlin GL, Donald AM (2007) Protein particulates: another generic form of protein aggregation? Biophys J 92:1336–1342

Lashuel HA, LaBrenz SR, Woo L, Serpell LC, Kelly JW (2000) Protofilaments, filaments, ribbons, and fibrils from peptidomimetic self-assembly: implications for amyloid fibril formation and materials science. J Am Chem Soc 122:5262–5277

Manno M, Craparo EF, Podestà A, Bulone D, Carrotta R, Martorana V, Tiana G, San Biagio PL (2007) Kinetics of different processes in human insulin amyloid formation. J Mol Biol 366:258–274

Manno M, Xiao C, Bulone D, Martorana V, San Biagio PL (2003) Thermodynamic instability in supersaturated lysozyme solutions: effect of salt and role of concentration fluctuations. Phys Rev E 68:011904

Militello V, Vetri V, Leone M (2003) Conformational changes involved in thermal aggregation processes of bovine serum albumin. Biophys Chem 105:133–141

Mine Y, Noutomi T, Haga N (1990) Thermally induced changes in egg white proteins. J Agric Food Chem 38:2122–2125

Muschol M, Rosenberger F (1997) Liquid–liquid phase separation in supersaturated lysozyme solution and associated precipitate formation/crystallization. J Chem Phys 107:1953–1962

Navarra G, Giacomazza D, Leone M, Militello V, San Biagio PL (2009) Pre-aggregates characterization and viscoelastic studies of BSA cold gels induced by metal ions. Eur Biophys J doi: 10.1007/s00249-008-0389-6

Nayakawa S, Nakamura R (1986) Optimization approaches to thermally induced egg white lysozyme gel. Agric Biol Chem 50:2039–2046

Nicolai T, Durand D, Gimel J-C (1996) Scattering properties and modelling of aggregating and gelling systems. In: Brown W (ed) Light scattering: principles and development. Clarendon Press, Oxford

Nohara D, Mizutani A, Sakai T (1999) Kinetic study on thermal denaturation of hen egg-white lysozyme involving precipitation. J Biosci Bioeng 87:199–205

Pace CN (1975) The stability of globular proteins. CRC Crit Rev Biochem 3:1–43

Panouille M, Nicolai T, Durand D (2004) Heat induced aggregation and gelation of casein submicelles. Int Dairy J 14:297–303

Pedersen JS (1993) Small-angle scattering from precipitates: analysis by use of a polydisperse hard-sphere model. Phys Rev B 47:657–665

Poon WCK, Egelhaaf SU, Beales PA, Salonen A, Sawyer L (2000) Protein crystallization: scaling of charge and salt concentration in lysozyme solutions. J Phys Condens Matter 12:L569–L574

Povey JF, Smales CM, Hassard SJ, Howard MJ (2007) Comparison of the effects of 2,2,2-trifluoroethanol on peptide and protein structure and function. J Struct Biol 157:329–338

Privalov PL (1979) Stability of proteins: small globular proteins. Adv Protein Chem 33:167–241

Prusiner SB (1998) Prions. Proc Natl Acad Sci USA 95:13363–13383

Puertas AM, De Michele C, Sciortino F, Tartaglia P, Zaccarelli E (2007) Viscoelasticity and Stokes–Einstein relation in repulsive and attractive colloidal glasses. J Chem Phys 127:144906

Rosch TW, Errington JR (2007) Investigation of the phase behavior of an embedded charge protein model through molecular simulation. J Phys Chem B 111:12591–12598

Rouse PEJ (1953) A theory of the linear viscoelastic properties of dilute solutions of coiling polymers. J Chem Phys 21:1272–1280

Rueb CJ, Zukoski CF (1998) Rheology of suspensions of weakly attractive particles: approach to gelation. J Rheol 42:1451–1476

Sabulal B, Kishore N (1995) Differential scanning calorimetric study of the interactions of some stabilizing amino acids and oligopeptides with hen egg white lysozyme. J Chem Soc Faraday Trans 91(14):2101–2106

Salvetti G, Tombari E, Mikheeva L, Johari GP (2002) The endothermic effects during denaturation of lysozyme by temperature modulated calorimetry and an intermediate reaction equilibrium. J Phys Chem B 106:6081–6087

Tanford C, Epstein J (1954) The physical chemistry of insulin. I. Hydrogen ion titration curve of zinc-free insulin. J Am Chem Soc 76:2163–2169

ten Wolde PR, Frenkel D (1997) Enhancement of protein crystal nucleation by critical density fluctuations. Science 277:1975–1978

van der Plancken I, Van Loey A, Hendrickx ME (2006) Effect of heat-treatment on the physico-chemical properties of egg white proteins: a kinetic study. J Food Eng 75:316–326

Vetri V, Librizzi F, Leone M, Militello V (2007) Thermal aggregation of bovine serum albumin at different pH: comparison with human serum albumin. Eur Biophys J 36:717–725

Winter HH, Chambon F (1986) Analysis of linear viscoelasticity of a crosslinking polymer at the gel point. J Rheol 30:367–382

Yan H, Saiani A, Gough JE, Miller AF (2006) Thermoreversible protein hydrogel as cell scaffold. Biomacromolecules 7:2776–2782

Zhang S (2003) Fabrication of novel biomaterials through molecular self-assembly. Nat Biotechnol 21:1171–1178